Journal Pre-proof

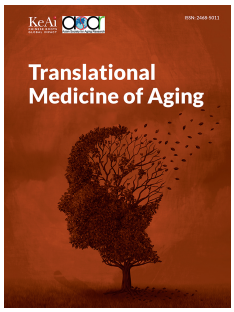

Remodeling of the H3 nucleosomal landscape during mouse aging

Yilin Chen, Juan I. Bravo, Jyung Mean Son, Changhan Lee, Bérénice A. Benayoun

PII: S2468-5011(19)30051-3

DOI: https://doi.org/10.1016/j.tma.2019.12.003

Reference: TMA 37

To appear in: *Translational Medicine of Aging*

Received Date: 28 August 2019

Revised Date: 14 December 2019

Accepted Date: 23 December 2019

Please cite this article as: Y. Chen, J.I. Bravo, J.M. Son, C. Lee, B.A. Benayoun, Remodeling of the H3 nucleosomal landscape during mouse aging, *Translational Medicine of Aging*, https://doi.org/10.1016/j.tma.2019.12.003.

Remodeling of the H3 nucleosomal landscape during mouse aging

Yilin Chen[1,2,+], Juan I. Bravo[1,3,+], Jyung Mean Son[1], Changhan Lee[1,4,5], and Bérénice A. Benayoun[1,4,6,*].

[1]Leonard Davis School of Gerontology, University of Southern California, Los Angeles, CA 90089, USA.

[2]Master of Science in Nutrition, Healthspan, and Longevity, University of Southern California, Los Angeles, CA 90089, USA.

[3]Graduate program in the Biology of Aging, University of Southern California, Los Angeles, CA 90089, USA.

[4]USC Norris Comprehensive Cancer Center, Epigenetics and Gene Regulation, Los Angeles, CA 90089, USA.

[5]Biomedical Sciences, Graduate School, Ajou University, Suwon 16499, Republic of Korea

[6]USC Stem Cell Initiative, Los Angeles, CA 90089, USA.

[+]equal contribution

[*]corresponding author

Corresponding Author's Information:

Bérénice A. Benayoun

+1 (213) 821-5997

berenice.benayoun@usc.edu

Abstract

In multi-cellular organisms, the control of gene expression is key not only for development, but also for adult cellular homeostasis, and deregulation of gene expression correlates with aging. A key layer in the study of gene regulation mechanisms lies at the level of chromatin: cellular chromatin states (*i.e.* the 'epigenome') can tune transcriptional profiles, and, in line with the prevalence of transcriptional alterations with aging, accumulating evidence suggests that the chromatin landscape is altered with aging across cell types and species. However, although alterations in the chromatin make-up of cells are considered to be a hallmark of aging, little is known of the genomic loci that are specifically affected by age-related chromatin state remodeling and of their biological significance. Here, we report the analysis of genome-wide profiles of core histone H3 occupancy in aging male mouse tissues (*i.e.* heart, liver, cerebellum and olfactory bulb) and primary cultures of neural stem cells. We find that, although no drastic changes in H3 levels are observed, local changes in H3 occupancy occur with aging across tissues and cells with both regions of increased or decreased occupancy. These changes are compatible with a general increase in chromatin accessibility at pro-inflammatory genes and may thus mechanistically underlie known shift in gene expression programs during aging.

1. Introduction

Precise control of gene expression is key not only for development in metazoans, but also for adult cellular homeostasis, and deregulation of gene expression correlates with aging [1-3]. Aging is the main risk factor for many chronic diseases, including neurodegeneration, cardiovascular disease, diabetes, and cancer. In eukaryotes, transcriptional profiles are regulated in part by chromatin states, which are notably governed by post-translational modifications of core histone proteins [4-9]. Interestingly, remodeling of chromatin landscapes, or so-called "epigenetic alterations" is considered to be a hallmark of aging [10, 11].

The overwhelming majority of core histone expression is restricted to the S-phase of the cell cycle [12], and post-mitotic or terminally differentiated cells show very little *de novo* synthesis [13]. Indeed, a number of canonical and variant histone proteins are among the longest-lived proteins in the proteomes of rat brain and liver, with stability in the order of months [14, 15]. Interestingly, core histone protein levels decrease during yeast replicative aging [16], and in mammalian models of cellular senescence [17]. Both of these paradigms are the results of repeated accumulated cell divisions. In addition, aged mouse muscle stem cells have lower transcript levels of several histone genes [18]. Substantial changes in histone expression level could lead to genome-wide remodeling of nucleosomal occupancy, and global changes in transcriptional outputs. Indeed, decreased histone expression during yeast replicative aging is linked to an overall decrease in nucleosome occupancy and the aberrant gene upregulation [19], and experimental modulation of histone exchange and deposition into chromatin, or overexpression of histone H3 and H4, can modulate *S. cerevisiae* lifespan [16]. Interestingly, even substantial loss of histone protein levels may lead to nucleosome occupancy changes at only a small number of genomic loci [20], thus suggesting that nucleosome occupancy may represent an important layer of gene expression regulation.

Local changes in nucleosome occupancy have previously been reported in the mouse aging liver using Micrococcal Nuclease treatment of chromatin followed by high-throughput sequencing [MNase-seq] (a method to map genome-wide nucleosome occupancy) [21], and these changes were proposed to facilitate the age-related activation of lipogenesis genes [21]. However, whether the observed remodeling results from changes in core histone expression or deposition patterns is still unclear. In addition, whether mammalian aging outside of highly replicative compartments is associated with histone loss throughout aging remains unknown.

Here, we present a reanalysis of H3 chromatin immunoprecipitation followed by high-throughput sequencing [ChIP-seq] datasets derived from a recent epigenomic study of male mouse aging across 4 tissues (*i.e.* heart, liver, cerebellum, olfactory bulb) and one primary cell type (*i.e.* primary neural stem cell cultures from the subventricular zone [NSCs]) at 3 ages throughout mouse lifespan (3, 12 and 29 months of age) [22]. Although we find evidence for neither widespread decrease in histone H3 expression levels with aging, nor for dramatic nucleosome occupancy changes with aging, we identify a number of robustly remodeled nucleosomes with mouse aging, including regions of both increased and decreased H3 occupancy. This analysis represents an important resource in the study of epigenomic remodeling during mammalian aging.

2. Results

2.1. Analysis of H3 ChIP-seq datasets reveals limited remodeling of H3 nucleosomes with aging

We took advantage of our previously obtained H3 ChIP-seq samples from aging male mouse tissue and cell samples to identify differentially regulated H3 nucleosome regions with aging [22] (**Fig. 1A**). To note, since no input libraries were generated in the previous study that we obtained the samples from [22], nucleosome calls reported here are respective to statistical background models from the DANPOS tool. The antibody used in these ChIP experiments (Abcam ab1791) is a polyclonal antibody that recognizes canonical and variant H3 protein, as well as modified and unmodified H3 versions, giving a global map of H3-bound sites in chromatin. This gold standard antibody in the epigenomics field was also used in previous studies of H3 levels in aging yeast [16] and fibroblast senescence [17], and is among the few validated antibodies for H3 founds in the antibody validation database [23].

Consistent with a previous study using MNase-seq on mouse aging liver tissue [21], we found that significant histone occupancy changes with mouse chronological aging were restricted to a limited number of loci (**Fig. 1B-D**). We were able to identify regions with both increased H3 occupancy or decreased H3 occupancy with aging (**Fig. 1B-D** and **S1A**), suggesting that a remodeling of both accessible and inaccessible regions occurs during aging. Regions with increased H3 occupancy with aging are expected to correspond to regions that are less accessible to the transcriptional machinery in aged tissues. Conversely, regions with decreased H3 occupancy with aging are expected to correspond to regions that are more accessible to the

transcriptional machinery in aged tissues. Both local increases and local decreases were identified throughout the mouse genome, without clustering to a specific chromosome (**Fig. 1C**). Thus, our analyses suggest that the H3 nucleosomal landscape of aging mammalian tissues is subjected to localized remodeling, with both regions of increased and decreased occupancy.

Because dramatic global changes in histone H3 protein levels could impact our ability to call remodeled nucleosomal regions, we assayed potential changes in H3 protein levels with aging using Western blotting in 2 of the same tissue types for which we reanalyzed ChIP-seq datasets: cerebellum and liver. We obtained tissues from young (5 months) and old (21 months) male C57BL/6N mice and extracted proteins from each tissue sample for analysis (**Fig. 2A**). Importantly, to account for non-biological variations in protein extraction efficiency, each tissue sample was split in 2 pieces and protein was extracted in parallel as technical duplicates (also see methods; **Fig. 2A**). We used the same H3 antibody for Western blot studies than the one that was used to generate the ChIP-seq datasets [22], as well as an antibody to histone H2B as an independent histone protein. Vinculin, a housekeeping cytoskeleton protein whose SDS-PAGE migration profile does not overlap with that of histones, was used a sample loading control in each Western blot analysis. Our analysis of protein levels in these tissues is consistent with an absence of large-scale changes in histone H3 protein expression levels with aging (**Fig. 2B,C,E,F** and **S2A,B,C**), and does not support the presence of consistent and dramatic decrease in histone H3 expression (or in histone H2B) with aging in mammalian tissues. Confirming our ability to detect robust changes in H3 levels, we were able to reproduce previously reported changes in total H3 levels in senescent fibroblasts [17] using 3 independent lines of human dermal fibroblasts (*i.e.* IMR-90, WI-38 and primary human dermal fibroblasts; **Fig. S3A-C**). Importantly, even when using a more sensitive and quantitative method to evaluate histone H3 protein levels in aging tissues (*i.e.* enzyme-linked immunosorbent assay [ELISA]), no significant trends for age-related changes in H3 levels in aging liver or cerebellum tissues were observed (**Fig. 2D,G**). Consistent with little change in H3 protein levels, our re-analysis of our previously published RNA-seq dataset in aging tissues [22] revealed no patterns of consistent directional changes in gene expression levels from all detectable genes encoding histone H3 (**Fig. S4A-E**). Indeed, detected transcripts derived from histone H3-encoding genes were observed to be unchanged, downregulated or upregulated with age (**Fig. S4A-E**). These observations are consistent with previous observations in an independent study of mouse liver aging [21].

Finally, we also recovered spike-in ChIP-seq reads mapping to the Drosophila genome in the total H3 ChIP-seq data [22, 24] (**Fig. S5**). Indeed, spike-in chromatin from Drosophila S2 cells was previously included in some of the published ChIP-seq samples [22], which can be used to evaluate global changes in chromatin association for an epitope of interest (*e.g.* H3 protein) by spiking a known, constant amount of chromatin from another species [24]. Thus, in the absence of global changes in H3 occupancy, the ratio of reads mapping to the genome of interest (*i.e.* here, the mm9 mouse assembly) normalized to reads mapping to the spike-in genome (*i.e.* here, the dm3 fly assembly) would be constant [24]. Consistent with the absence of a general decrease in H3 levels with aging, actual ChIP spike-in ratio values did not show robust or reproducible decreasing trends across tissues (**Fig. S5**). To note, although limited replicate numbers restrains our ability to apply statistical analysis to this data, trends for increased global H3 occupancy may be occurring in liver, with almost twice as many reads mapping to the mouse genome relative to those mapping to the fly genome in the young *vs.* old samples, consistent with the non-significant trend observed in liver Western blot (**Fig. 2C**, and **S2A**) but not by ELISA.

Taken together, our analyses suggest that, in contrast to replicatively aged yeast [16] or senescent mammalian cells [17], core histone expression levels are not dramatically nor consistently decreasing in chronologically aging mammalian tissues.

2.2 Age-related changes in H3 occupancy are frequent at distal elements, and enriched at intronic regions

Next, we analyzed the genomic distribution of nucleosome with age-related decreased (Fig. 3A) or increased H3 occupancy across tissues. The relative distances of these remodeled nucleosomes to annotated TSSs are indicated in **Fig. 3A-B** (*i.e.* >500kp away from TSS, 500-50kb, 50-5kb, 5-0kb in both directions, indicated on the genomic axis below the bars). Significantly remodeled regions of H3 occupancy tended to occur most often at distal regions, 5 to 500 kb away from annotated transcriptional start sites [TSS] both upstream and downstream (**Fig. 3A-B**). This observation is consistent with previous observations of age-related nucleosomal occupancy changes in aging livers between 3 and 21 months of age using MNase-seq [21], which we now also extend to heart, cerebellum, olfactory bulb and primary NSCs.

In all tissue samples, when compared to the genomic distribution of all detected nucleosomes in our samples, sites proximal to genes, especially in intronic regions, were robustly

and consistently overrepresented compared to background nucleosomes (**Fig. 3C-D** and **S1B-E**; **Supplementary Table S1A-B**). Importantly, we specifically used as a background control the set of background nucleosomes detected by DANPOS, rather than the entire genome sequence, to avoid biases from regions of the genome inaccessible to analysis for technical reasons (*e.g.* repetitive sequences with poor mapability, which represent >30% of the mouse genome). To quantify the significance of putative enrichments, we randomly sampled nucleosomes from the pool of detected nucleosomes by DANPOS in each tissue and used the HOMER pipeline to annotate them to genomic elements. Interestingly, we found that such an enrichment at intronic sites was unlikely to occur by chance ($p < 0.004$ based on results from 250 random samples) (**Supplementary Table S1B**). To note, this phenomenon was much less pronounced in the NSCs samples, which harbor much less genomic age-related changes in general [22]. Other genomic elements (*e.g.* promoters) were not as robustly and significantly enriched over background across tissues (**Supplementary Table S1B**).

Our observations that most changed nucleosomes occur distally may indicate differential occupancy of regulatory elements (*e.g.* enhancers, silencers) in aging chromatin context. In addition, we observed a slight trend for regions with remodeled H3 occupancy to fall within regions proximal or overlapping genes (*i.e.* introns, proximal promoter, coding exons, 5' and 3' untranslated regions) more often than compared to background detected nucleosomes (**Fig. 3C-D**, and **S1B-E**; **Supplementary Table S1A-B**). This may suggest that lifelong patterns of transcriptional activity may ultimately lead to genomic remodeling of H3 occupancy. Although informative, genome ontology analysis does not provide information on the function or activity of annotated elements. Chromatin-state annotation using combinations of chromatin modification patterns is a powerful approach to annotate tissue-specific activity patterns of regulatory regions [25, 26]. To understand the chromatin context at regions with age-remodeled H3 occupancy, we leveraged the widely used chromHMM algorithm [25, 26]. This algorithm uses chromatin mapping datasets to learn genome-wide chromatin states maps, using ChIP-seq data from our previous study [22], the mouse ENCODE project [27] and other available datasets in tissues/cell of interest (see **Supplementary Table S2A-C** for all genomic dataset accession numbers). Specific chromatin states learned by the algorithm were annotated to families of regulatory elements (*e.g.* enhancer, gene body, etc.) based on the co-occurrence pattern of each chromatin feature in these states [25, 26] (**Figure S6A-G**). We then compared the genome positions of

remodeled nucleosomes to that of mapped "youthful" chromatin states (**Supplementary Table S1C-D**). Interestingly, outside of "low signal" regions (which are likely unexpressed gene deserts), the majority of age-remodeled nucleosomes were found to reside in weak/poised enhancers in young chromatin (**Supplementary Table S1C-D**), consistent with coordinated chromatin remodeling at facultative regulatory regions during aging.

2.3 Differential enrichment of putative regulatory motifs is consistent with increased accessibility of pro-inflammatory gene programs

To understand the potential biological significance of remodeled regions of H3 occupancy in aging mouse tissues, we leveraged the GREAT annotation portal [28], an online toolkit which allows functional annotation of genomic regions rather than genes (**Supplementary Table S3**). Here, we focused on the annotation "Molecular Signature Database motifs enriched at promoters" to identify potential associations to differential transcription factor behaviors (**Fig. 4A-B**). The majority of motifs associated to changed regions that were recurrently enriched (*i.e.* in 3 or more datasets) were linked to Forkhead transcription factors [TFs] (*e.g.* FOXO4, FOXF2, FOXL1, FOXA1, etc.), both at regions of increased and decreased H3 occupancy (**Fig. 4A-B**). These observations are consistent with the previous MNase-seq analysis of aging liver [21], and show that remodeling of Forkhead TF regulated sites may be a general features of chromatin accessibility during aging. Interestingly, Forkhead TFs can act as 'pioneer' factors and directly remodel chromatin; for example, Foxo1 and Foxa2 are able to bind nucleosomal DNA, and lead to chromatin decompaction [29, 30]. FOXO factors are known to act as pro-longevity genes [31], and may thus help remodel relevant chromatin regions during the aging process. Interestingly, in the RNA-seq dataset associated with the original publication of this genomic resource [22], transcriptional targets of Forkhead TFs (*i.e.* FOXO1, FOXO3, FOXO4, FOXA1 and FOXA2) were found to be significantly transcriptionally upregulated with aging [22], consistent with the notion that Forkhead TF transcriptional target networks may be remodeled downstream of chromatin remodeling during aging.

Consistent with the overall 'omic' signature of inflammatory response with age at the transcriptomic and histone modification levels [22], regions with decreased H3 occupancy (*i.e.* regions likely to be more accessible and active with aging) were recurrently enrichment for association with inflammation-related TF motifs (**Fig. 4A**), including motifs associated with

IRF1, STAT6 and TCF3. Consistently, transcriptional targets of IRF8 and TCF3 were previously noted to be significantly upregulated with aging across tissues [22]. Thus, chromatin remodeling at the levels of nucleosomal occupancy may be partially coordinated by inflammatory TFs, thus leading to increased accessibility of key regulatory regions of inflammatory genes, and mechanistically underlie the induction of innate immune response pathways with aging.

3. Discussion

In conclusion, to understand the effect of aging on nucleosome occupancy with aging, we reanalyzed transcriptomic and epigenomic maps in young, middle-aged, and old mice from a variety of tissues and cells known to show functional decline with aging (*i.e.* heart, liver, cerebellum, olfactory bulb and primary cultures of NSCs) [22]. We also complemented the genomic study with measurements of total histone H3 protein levels in aging tissues using Western blotting and ELISA. To our knowledge, this study represents the most comprehensive analysis of histone expression and occupancy changes with mammalian aging to date. We hope that it will serve as a resource for the aging research community. To note, although no drastic global changes were observed across all tissues in terms of histone expression levels were observed, our analysis reveals the importance of including nucleosome occupancy as a control for histone modification studies. Indeed, with the use of traditional input controls, changes in local histone occupancy may mask (or aberrantly reveal) true changes in local histone post-translation modification patterns.

Based on our observations and previously published reports, it is likely that dramatically decreased nucleosome occupancy only occurs in a cell-type- or context-specific manner with aging and is not the rule in mammalian tissues. It is also possible that MNase and ChIP-seq based methods may not be sensitive enough to detect subtle distribution changes, which may become detectable with higher-resolution methods which could be unveiled with future study. However, motifs enriched in regulatory regions of genes with remodeled nucleosomal occupancy revealed potential regulation by multiple inflammatory transcription factors, such as STAT6 and IRF8, which is consistent with transcriptional trends observed with aging [22]. Thus, changes in underlying accessibility of DNA to transcription factors may play a mechanistic role in the activation of inflammatory gene programs during mammalian aging.

In this study, we profiled "total H3", which encompasses all cellular versions of H3 (*i.e.* canonical and variants). We note that, in addition to canonical histone genes, the transcription of which is usually restricted to S-phase, some histone variants (including H3 variants) can be expressed throughout the cell cycle [2]. These specific variants may be involved in gene expression regulation (*e.g.* H3.3) or chromatin structure (*e.g.* CENP-A) [32]. Importantly, chromatin organization and function can be affected by changes in core histone expression, incorporation of functional histone variants or the activity of nucleosome remodelers, which are all relevant to the aging process [2]. A number of histone variants (*e.g.* H3.3, macroH2A) that can replace canonical histones in the chromatin fiber have distinct genomic profiles of incorporation, and are thought to have structural or regulatory impact [33]. A specific variant of histone H3, named H3.3, has been gathering particular interest in the context of aging [34]. Consistent with H3.3 expression being independent of cell cycle, unlike its canonical H3.1 and H3.2 counterparts, the H3.3 histone variant progressively accumulates in metazoan cells and tissues with age [35-38], and in senescent cells [39 , 40]. Although antibodies with high affinity and specificity for H3.3 are not readily available and validated yet, future work studies disentangling the relative presence of specific H3 variants may further explain age-related gene dysregulation, and will be important to interrogate in the future.

In the long-term, understanding not only changes in histone post-translational modification patterns, but also changes in the underlying distribution of histones on the chromatin throughout life and in response to various stimuli will be key in understanding novel aspects of the "histone code" [4] regulation of biological processes.

4. Materials and Methods

Mouse husbandry

All animals were treated and housed in accordance to the Guide for Care and Use of Laboratory Animals. All experimental procedures were approved by USC's Institutional Animal Care and Use Committee (IACUC) and were in accordance with institutional and national guidelines. Male C57BL/6N mice at different ages were obtained from the National Institute on Aging (NIA) aging colony at Charles Rivers. Mice were acclimated at the animal facility at USC for 2-4 weeks before euthanasia. All animals were euthanized between 9am-12pm, and a variety

of tissues were collected, snap frozen in liquid nitrogen, and stored at −80°C until further handling. No live animals were censored.

Preparation of protein samples

Proteins were extracted from frozen liver and cerebellum samples. Each sample was split in two portions in order to carry out two independent protein extractions. At the times of protein extraction, tissues were maintained on ice, cut, and transferred to MP Biomedicals Lysing Matrix D tubes (MP Biomedicals #MP116913050) containing 1X RIPA Lysis Buffer (Millipore #20-188) and 1X Halt Protease and Phosphatase Inhibitors (Thermo-Fisher Scientific #78440). Tissues were homogenized (1 cycle for cerebellums; 3 cycles for livers of 30 seconds at 3500 rpm), and lysates were centrifuged to remove debris and insoluble fraction at 10,000g and 4°C for 10 min. The supernatants were used as tissue protein lysates. Liver samples were centrifuged an additional time before collecting lysates in order to minimize fat transfer. Protein lysate concentrations were quantified using the Pierce BCA Protein Assay Kit (Thermo-Fisher Scientific #23227) following manufacturer's instructions. Lysates were diluted to the same final protein concentration, mixed with 2X or 4X Laemmli sample buffer (Biorad #1610737) supplemented with 2-mercaptoethanol (Sigma # 60-24-2), and denatured by boiling at 95°C for 10 min.

Senescent fibroblast generation and protein extraction

Human fibroblast cell lines IMR-90 (I90-83), WI-38 (AG06814 N) and normal human dermal fibroblasts [HDF] (AG16409A) were obtained from the Coriell Cell Repositories – Coriell Institute for Medical Research. IMR-90 and WI-38 cell lines were cultured in MEM with Earle's Salts and L-Glutamine (Corning #10-010-cv), supplemented with 15% Fetal Bovine Serum (Sigma #F0926), 1X Penicillin/Streptomycin (Corning #30-002-CI) and 1X MEM-NEAA (Quality Biological #116-078-721). Healthy skin fibroblasts were cultured in DMEM (Corning Cat# 10-017-CV), supplemented with 10% Fetal Bovine Serum (Sigma #F0926). All cells were incubated in a humidity-controlled environment at 37°C, 5% CO_2. Asynchronously growing cells were used at respectively passages 9-11 (IMR-90), 19-21 (WI-38) and 10-11 (HDF). Doxorubicin hydrochloride (Sigma #D1515) was used for genotoxic stress-induced senescence. Senescence was induced by exposure to 250nM Doxorubicin for 24h [41, 42]. After treatment, cells were

washed twice with 1xPBS, and returned to their standard doxorubicin-free culture medium for 14 days, during which culture medium was replaced with fresh medium every 3 days. For IMR-90 and WI-38 cells, senescent status was confirmed with paired control and treated samples probed for SA-β-galactosidase signal (Cell Signaling Technology #9860) (**Fig. S3A**). Protein extracts were obtained using RIPA supplemented with protease inhibitors similar to tissue samples (see above).

SDS-PAGE and Western Blot

For the set of liver samples probed for H3, polyacrylamide gels were prepared with a 5% stacking layer (388 mM Tris pH 8.8, 4% Acrylamide:Bis 29:1, 1% SDS, 1% APS, 0.1% TEMED) and a 10% separating layer (388 mM Tris pH 8.8, 10% Acrylamide:Bis 29:1, 0.9% SDS, 0.9% APS, 0.04% TEMED) in Mini-PROTEAN cassettes (Biorad #4560005). For all other samples, 4–20% Mini-PROTEAN TGX Precast Protein Gels (Biorad #4561095) were used. Electrophoresis cells were filled with 1X Tris-Glycine-SDS Running Buffer (Bioland) before loading gels with 30µg (tissue samples) or 7.5µg (cell samples) of protein per well. Precision Plus Protein Standards (Biorad #161-0374) were used to track protein mass. Gels were prepared in duplicates, one for transferring onto PVDF Blotting Membrane (Sigma), and one for total protein staining by Coomassie blue following manufacturer recommendations (Biorad #1610436, 1610438). Protein transfers were conducted in Transfer buffer (48mM Tris base, 39mM Glycine, 1.28mM SDS, 20% Ethanol) at 4°C for 1 hour with 250 mA of constant current. After transfer, membranes were blocked with 5% Bovine Serum Albumin [BSA] (AK8917-0100) in Tris-buffered saline [TBS] (J62938) (liver) or TBS-0.1% Tween [TBS-T] (cerebellum, IMR-90, WI-38, and HDF) for 1 hour. All primary and secondary antibodies were prepared using 5% BSA in TBS-T.

After blocking, membranes were cut based on the molecular mass as indicated by protein standards to allow for simultaneous detection of proteins of different molecular weight, and incubated overnight at 4°C with Anti-Vinculin antibody (used as gel loading control and normalization reference; 1:2,000, Abcam ab91459), Anti-Histone H3 antibody (1:1,000 for liver and 1:5,000 for cerebellum, IMR-90, WI-38, and HDF; Abcam ab1791), or Anti-Histone H2B antibody (1:10,000 for both liver and cerebellum, Abcam ab1790), based on the expected molecular weights of the proteins to be assayed. Abcam ab1791 is expected to recognize all

versions of H3 (*i.e.* canonical and variants, modified and unmodified), through a common region at the protein sequence level which is targeted by this antibody. Although further validation of the antibody is beyond the scope of our study, this antibody is the gold standard in the epigenomics field. In addition, this same antibody was used in previous studies of H3 levels in aging yeast [16] and senescent fibroblasts [17], and is among the few validated antibodies for H3 founds in the antibody validation database [23]. Membranes were then washed with TBST three times and incubated with Goat Anti-Rabbit IgG H&L (HRP) secondary antibody 1:10,000 dilution (Abcam ab205718) for 1 hour at room temperature. Membranes were washed with TBST three times before incubating with SuperSignal West Pico PLUS Chemiluminescent Substrate (Thermo-Fisher Scientific #34580) for 5 minutes. Protein signals were detected using an Azure c280 imaging system. Protein band quantifications were conducted using the gel analysis module of the ImageJ software, and for each tissue sample, the average of 2 technical replicates for protein extraction are reported as one data point. Data was plotted and statistical analysis was performed using the R statistical software.

Total H3 quantification in mouse tissue protein extract using ELISA

For quantitative evaluation of H3 levels in aging cerebellum and liver samples, we used the RIPA protein extracts from non-gradient cohorts as above. We performed ELISA quantification of H3 levels using Abcam's Histone H3 Total Quantification Kit (ab115091), with a few modifications from the manufacturer's protocol to accommodate whole cell extracts rather than histone extracts. All samples were diluted to the target concentration in 1X RIPA Lysis Buffer (Millipore #20-188) and 1X Halt Protease and Phosphatase Inhibitors (Thermo-Fisher Scientific #78440), to a target of 50ug of total protein per well. To account for potential impact of this buffer on the ELISA assay, the H3 protein standard was also diluted in the same RIPA volume as the samples. A paired plate was used for BCA quantification (Pierce BCA Protein Assay Kit # 23225) in parallel to the ELISA assays following manufacturer's instructions, in order to normalize each well to actual protein levels in each well. Technical replicates, corresponding to the 2 independent extractions on tissue from the same animal as above, were averaged before plotting and statistical analysis.

ChIP-Seq data processing

H3 ChIP-seq data was obtained from the NCBI Short Read Archive (SRA) accession SRP057387 (BioProject PRJNA281127) and processed as explained previously in the original manuscript describing the ChIP-seq dataset [22]. Briefly, sequencing reads were trimmed using Trimgalore v0.3.1 (https://github.com/FelixKrueger/TrimGalore) to retain high-quality bases with Phred quality scores >15 and a post-trimming length of 36bp. Reads were mapped to the genome using bowtie version 0.12.7. PCR duplicates were removed using FIXseq (fixseq-e2cc14f19764) [43]. All ChIP-seq dataset accession numbers can be found in **Supplementary Table S2**.

Nucleosome mapping and remodeling analysis

Total H3 ChIP-seq data was used to assess changes in nucleosome occupancy with aging. Nucleosome site calls are derived from our previous study [22]. To note, because that study did not include input samples, calls are against the statistical background model of the DANPOS tool. Briefly, since existing pipelines do not have time-series capability, we performed analyses comparing the young (3m) and old (29m) samples in each tissue type to assess the impact of aging. Differential occupancy position between 3 and 29 months were independently called using the DANPOS (danpos v2.2.2) (p-value < 10^{-15}) [44] and DiNup (dinup v1.3) (False Discovery Rate [FDR] < 5%) algorithms [45]. Only positions called as differential by both algorithms were considered as robustly changing with age and further analyzed.

Analysis of genomic distribution of remodeled regions

Significant regions of interest (*i.e.* nucleosomes) were annotated to the gene with the closest transcription start site using HOMER [46]. We extracted and plotted the distance between the region of interest and closest annotated transcription start site [TSS] in the mm9 mouse genome build (**Fig. 3A,B**). Basic genome ontology analysis was also performed with HOMER. The relative enrichment of remodeled regions compared to genomic elements was performed using the Cis-regulatory Element Annotation System [CEAS] software v1.0.2 [47] (**Fig. S1B-E; Supplementary Table S1A**). Fold difference with respect to the background nucleosomes annotated in the same fashion is reported (**Fig. 3C-D; Supplementary Table S1A**). To evaluate whether enrichment at specific genomic elements may be statistically significant, 250 random samples of detected nucleosomes in the tissue/cell of interest were obtained and annotated to

genomic elements using HOMER's Genome Ontology annotation module [46] (as CEAS cannot produce easily computer-readable outputs from such large amount of input files). The empirical cumulative distribution function (eCDF) over these samples was compared to the real observed enrichments, to obtain an empirical p-value of enrichments expressed as 1-(percentile of the real value). All of the calculated empirical enrichments and p-values are reported in **Supplementary Table S1B**.

Analysis of histone gene expression in RNA-seq data

DEseq2 normalized RNA-seq expression count tables were derived from our previous study [22]. Official gene symbol for histone genes were obtained from ENSEMBL BioMart on 2019-07-23, and genes encoding core or variants of histone H3 were selected for further analysis. Genes were considered to be detectable if at least 1 read was detected across all samples in that specific tissue. Expression for detectable histone H3 genes was then reported as a boxplot for each age, shown in **Fig. S4A-E**.

Model building for chromatin states analyses with chromHMM

To train chromHMM models [25, 26], we obtained ChIP-seq datasets (*i.e.* H3K4me3, H3K27ac, H3K4me1, H3K27me3, Pol2, CTCF and DNAse/ATAC) in the studied mouse tissues [48] and in cultured NSCs [22, 49, 50]. Mapped sequencing reads were fed to the chromHMM v1.12 algorithm to learn 10 states across the 5 conditions (*i.e.* heart, liver, cerebellum, olfactory bulb and NSCs). Chromatin state predictions were generated using ChromHMM v1.12 [25, 26]. The model was built using H3K4me3, H3K27ac, H3K4me1, H3K27me3, Pol2, CTCF and DNAse/ATAC from young adult samples (see **Supplementary Table S2** for all genomic dataset accession numbers). Default parameters were used for the HMM training. For prediction of states, a 10-state model was empirically determined to most closely represent the expected states (*e.g.* promoter-like states found near TSSs). The final emission properties learned by ChromHMM are reported in **Fig. S6A-G**. We calculated the overlap of learned chromatin states with significantly remodeled nucleosomes (**Supplementary Table S1C)**. In addition, for ease of interpretation, similar chromatin states were subsequently merged, resulting in 8 summarized main states: low signal, active enhancer, weak/poised enhancer, inactive/poised promoter,

polycomb repressed, insulator, active promoter, and flanking promoter (**Supplementary Table S1D**).

Functional enrichment analysis of remodeled regions using GREAT

Functional term enrichment analysis was conducted by comparing differentially enriched H3 regions to all detected H3 regions using the GREAT v3.0.0 online functional annotation tool [28]. Genomic coordinates of peaks (in the form of bed files) were used. For ease of graphical representation, terms enriched in at least 3 of the 5 conditions at FDR < 10^{-6} were selected for analysis and plotting (**Fig. 4A-B**). All enriched terms are reported in **Supplementary Table S3A-B**.

Code Availability

All the new analytical code from this study is available on the Benayoun laboratory Github repository (https://github.com/BenayounLaboratory/Nucleosome_aging_2019).

Acknowledgements

J.B. was supported by NIA T32AG052374 and NSF graduate research fellowship DGE-1842487. J.M.S. and C.L. are supported by NIA R01AG052558. B.A.B is supported by NIA R00AG049934, an innovator grant from the Rose Hills foundation, a seed grant from the NAVIGAGE foundation, and a generous gift from the Hanson-Thorell Family. The authors thank members of the Benayoun, Vermulst and Lee labs for helpful discussions and feedback.

Conflict of interest

The authors declare that they have no conflict of interest to disclose.

References

1. Benayoun, B.A., E.A. Pollina, and A. Brunet, *Epigenetic regulation of ageing: linking environmental inputs to genomic stability.* Nat Rev Mol Cell Biol, 2015. **16**(10): p. 593-610.
2. Ucar, D. and B.A. Benayoun, *Chapter 1 - Aging Epigenetics: Changes and Challenges*, in *Epigenetics of Aging and Longevity*, A. Moskalev and A.M. Vaiserman, Editors. 2018, Academic Press: Boston. p. 3-32.
3. Lai, R.W., et al., *Multi-level remodeling of transcriptional landscapes in aging and longevity.* BMB Rep, 2019. **52**(1): p. 86-108.
4. Jenuwein, T. and C.D. Allis, *Translating the histone code.* Science, 2001. **293**(5532): p. 1074-80.
5. Dunham, I., et al., *An integrated encyclopedia of DNA elements in the human genome.* Nature, 2012. **489**(7414): p. 57-74.
6. Whyte, Warren A., et al., *Master Transcription Factors and Mediator Establish Super-Enhancers at Key Cell Identity Genes.* Cell, 2013. **153**(2): p. 307-319.
7. Parker, S.C., et al., *Chromatin stretch enhancer states drive cell-specific gene regulation and harbor human disease risk variants.* Proc Natl Acad Sci U S A, 2013. **110**(44): p. 17921-6.
8. Dong, X., et al., *Modeling gene expression using chromatin features in various cellular contexts.* Genome biology, 2012. **13**(9): p. R53.
9. Hoffman, M.M., et al., *Integrative annotation of chromatin elements from ENCODE data.* Nucleic acids research, 2012: p. gks1284.
10. Kennedy, B.K., et al., *Geroscience: linking aging to chronic disease.* Cell, 2014. **159**(4): p. 709-13.
11. Lopez-Otin, C., et al., *The hallmarks of aging.* Cell, 2013. **153**(6): p. 1194-217.
12. Whitfield, M.L., et al., *Stem-loop binding protein, the protein that binds the 3' end of histone mRNA, is cell cycle regulated by both translational and posttranslational mechanisms.* Mol Cell Biol, 2000. **20**(12): p. 4188-98.
13. Lyons, S.M., et al., *A subset of replication-dependent histone mRNAs are expressed as polyadenylated RNAs in terminally differentiated tissues.* Nucleic Acids Res, 2016. **44**(19): p. 9190-9205.
14. Savas, J.N., et al., *Extremely long-lived nuclear pore proteins in the rat brain.* Science, 2012. **335**(6071): p. 942.
15. Toyama, B.H., et al., *Identification of long-lived proteins reveals exceptional stability of essential cellular structures.* Cell, 2013. **154**(5): p. 971-82.
16. Feser, J., et al., *Elevated histone expression promotes life span extension.* Mol Cell, 2010. **39**(5): p. 724-35.
17. O'Sullivan, R.J., et al., *Reduced histone biosynthesis and chromatin changes arising from a damage signal at telomeres.* Nat Struct Mol Biol, 2010. **17**(10): p. 1218-25.
18. Liu, L., et al., *Chromatin modifications as determinants of muscle stem cell quiescence and chronological aging.* Cell reports, 2013. **4**(1): p. 189-204.
19. Hu, Z., et al., *Nucleosome loss leads to global transcriptional up-regulation and genomic instability during yeast aging.* Genes Dev, 2014. **28**(4): p. 396-408.
20. Celona, B., et al., *Substantial histone reduction modulates genomewide nucleosomal occupancy and global transcriptional output.* PLoS Biol, 2011. **9**(6): p. e1001086.

21. Bochkis, I.M., et al., *Changes in nucleosome occupancy associated with metabolic alterations in aged mammalian liver.* Cell Rep, 2014. **9**(3): p. 996-1006.
22. Benayoun, B.A., et al., *Remodeling of epigenome and transcriptome landscapes with aging in mice reveals widespread induction of inflammatory responses.* Genome Res, 2019. **29**(4): p. 697-709.
23. Egelhofer, T.A., et al., *An assessment of histone-modification antibody quality.* Nature Structural & Molecular Biology, 2011. **18**(1): p. 91-93.
24. Orlando, D.A., et al., *Quantitative ChIP-Seq normalization reveals global modulation of the epigenome.* Cell Rep, 2014. **9**(3): p. 1163-70.
25. Ernst, J. and M. Kellis, *Chromatin-state discovery and genome annotation with ChromHMM.* Nature Protocols, 2017. **12**: p. 2478.
26. Ernst, J. and M. Kellis, *ChromHMM: automating chromatin-state discovery and characterization.* Nature Methods, 2012. **9**: p. 215.
27. Yue, F., et al., *A comparative encyclopedia of DNA elements in the mouse genome.* Nature, 2014. **515**(7527): p. 355-64.
28. McLean, C.Y., et al., *GREAT improves functional interpretation of cis-regulatory regions.* Nat Biotechnol, 2010. **28**(5): p. 495-501.
29. Hatta, M. and L.A. Cirillo, *Chromatin opening and stable perturbation of core histone:DNA contacts by FoxO1.* The Journal of biological chemistry, 2007. **282**(49): p. 35583-93.
30. Li, Z., et al., *The nucleosome map of the mammalian liver.* Nat Struct Mol Biol, 2011. **18**(6): p. 742-6.
31. Martins, R., G.J. Lithgow, and W. Link, *Long live FOXO: unraveling the role of FOXO proteins in aging and longevity.* Aging Cell, 2016. **15**(2): p. 196-207.
32. Maze, I., et al., *Every amino acid matters: essential contributions of histone variants to mammalian development and disease.* Nature reviews. Genetics, 2014. **15**(4): p. 259-71.
33. Zink, L.M. and S.B. Hake, *Histone variants: nuclear function and disease.* Curr Opin Genet Dev, 2016. **37**: p. 82-9.
34. Saade, E., et al., *Molecular turnover, the H3.3 dilemma and organismal aging (hypothesis).* Aging Cell, 2015. **14**(3): p. 322-33.
35. Piazzesi, A., et al., *Replication-Independent Histone Variant H3.3 Controls Animal Lifespan through the Regulation of Pro-longevity Transcriptional Programs.* Cell Rep, 2016. **17**(4): p. 987-996.
36. Urban, M.K. and A. Zweidler, *Changes in nucleosomal core histone variants during chicken development and maturation.* Dev Biol, 1983. **95**(2): p. 421-8.
37. Pina, B. and P. Suau, *Changes in histones H2A and H3 variant composition in differentiating and mature rat brain cortical neurons.* Dev Biol, 1987. **123**(1): p. 51-8.
38. Wu, R.S., S. Tsai, and W.M. Bonner, *Changes in histone H3 composition and synthesis pattern during lymphocyte activation.* Biochemistry, 1983. **22**(16): p. 3868-73.
39. Rai, T.S., et al., *HIRA orchestrates a dynamic chromatin landscape in senescence and is required for suppression of neoplasia.* Genes Dev, 2014. **28**(24): p. 2712-25.
40. Duarte, L.F., et al., *Histone H3.3 and its proteolytically processed form drive a cellular senescence programme.* Nat Commun, 2014. **5**: p. 5210.
41. Demaria, M., et al., *Cellular Senescence Promotes Adverse Effects of Chemotherapy and Cancer Relapse.* Cancer Discov, 2017. **7**(2): p. 165-176.
42. Kim, S.J., et al., *Mitochondrial peptides modulate mitochondrial function during cellular senescence.* Aging (Albany NY), 2018. **10**(6): p. 1239-1256.

43. Hashimoto, T.B., M.D. Edwards, and D.K. Gifford, *Universal count correction for high-throughput sequencing.* PLoS Comput Biol, 2014. **10**(3): p. e1003494.
44. Chen, K., et al., *DANPOS: dynamic analysis of nucleosome position and occupancy by sequencing.* Genome Res, 2013. **23**(2): p. 341-51.
45. Fu, K., et al., *DiNuP: a systematic approach to identify regions of differential nucleosome positioning.* Bioinformatics, 2012. **28**(15): p. 1965-71.
46. Heinz, S., et al., *Simple combinations of lineage-determining transcription factors prime cis-regulatory elements required for macrophage and B cell identities.* Mol Cell, 2010. **38**(4): p. 576-89.
47. Shin, H., et al., *CEAS: cis-regulatory element annotation system.* Bioinformatics, 2009. **25**(19): p. 2605-6.
48. Yue, F., et al., *A comparative encyclopedia of DNA elements in the mouse genome.* Nature, 2014. **515**(7527): p. 355-364.
49. Webb, A.E., et al., *FOXO3 shares common targets with ASCL1 genome-wide and inhibits ASCL1-dependent neurogenesis.* Cell Rep, 2013. **4**(3): p. 477-91.
50. Phillips-Cremins, J.E., et al., *Architectural protein subclasses shape 3D organization of genomes during lineage commitment.* Cell, 2013. **153**(6): p. 1281-95.
51. Howe, C.G. and M.V. Gamble, *Enzymatic cleavage of histone H3: a new consideration when measuring histone modifications in human samples.* Clin Epigenetics, 2015. **7**: p. 7.
52. Yi, S.J. and K. Kim, *Histone tail cleavage as a novel epigenetic regulatory mechanism for gene expression.* BMB Rep, 2018. **51**(5): p. 211-218.

Figure Legends

Figure 1: The genome wide H3 nucleosomal landscape of mouse aging in four tissues and one cell type

(A) Experimental and analytical data setup from [22]. (B) UCSC Genome Browser Shots for examples of significantly remodeled nucleosomal regions in the liver (Top) or cerebellum (Bottom) samples. chr: chromosome. Coordinates are relative to the mm9 genome build. (C) Circular genome plot showing the genomic distribution of significantly remodeled H3 nucleosomes in Heart (a), Liver (b), Cerebellum (c), Olfactory Bulb (d) and primary NSC cultures from the subventricular zone [SVZ] (e). Note that there is no obvious clustering on specific chromosomes. Because the X and Y chromosomes are hemizygote in males, they are assessed at a lower depth than autosomes and thus lower statistical power to call differential occupancy, which may explain the observed lower density of remodeled nucleosomes on the sex chromosomes that we. (D) Barplot of frequencies of regions with increased (red) or decreased (blue) H3 occupancy with aging. The percentage of nucleosomes with increased or decreased occupancy relative to all detected nucleosomes is reported next to the bar.

Figure 2: Analysis of H3 protein levels in aging mouse liver and cerebellum samples by Western blot.

(A) Schematic illustrating experimental setup and methodology for histone quantification in aging liver and cerebellum tissue. (B,E) Representative western blot images for Vinculin (loading control), total H3 and H2B in liver (B) and cerebellum (E) protein extract. All western blots are available in **Figure S2**. (C,F) Quantification of H3 and H2B relative protein intensity using Western Blots from 5 *vs.* 21 months tissues (normalized to cognate Vinculin loading control). The average relative protein intensity of the technical extraction/blotting replicates for each animal are reported as one data point. All quantified gels are annotated and provided in **Figure S2A-B**, and all quantified raw Western blot images are also available as a supplemental archive file. Note that a faster migrating band can be observed in some H3 western blots. This band is generally fainter than the higher H3 molecular weight band observed, and may correspond to previously reported H3 cleavage [51, 52]. For simplicity purposes, as relative quantities of both bands co-vary, we only report quantification of the stronger band in panels C and F. Results are reported normalized to the respective intensity of the Vinculin band, and then, to correct for

cohort-to-cohort variations, to the median value in the cognate cohort (each cohort is represented by dots in a different color). (D,G) ELISA quantification of H3 protein content relative to total protein as measured by BCA in aging Liver (D) or Cerebellum (G) protein extracts. P-values reported above boxplots were obtained with the non-parametric Mann-Whitney/Wilcoxon test.

Figure 3: Genomic localization of age-remodeled nucleosomes

(A-B) Relative distance to annotated transcription start sites [TSSs] of nucleosomes with decreased (A) and increased (B) H3 occupancy during mouse aging. The relative distances of remodeled nucleosomes to annotated TSSs are indicated along an axis of distance to TSS (*i.e.* >-500kp away from closest TSS, -500 to -50kb, -50 to -5kb, -5kb to TSS, TSS to +5kb, +5 to +50kb, +50 to +500kb and >+500kb from closest TSS). (C-D) Fold enrichment for remodeled nucleosomes to occur at various genomic sites by CEAS compared to background detected nucleosomes for nucleosomes with decreased (C) or increased (D) H3 occupancy during mouse aging. Absolute numbers and empirical statistical enrichments are reported in **Fig. S1B-E** and **Supplementary Table S1A,B**.

Figure 4: Enrichment of putative transcription factor targets for genes associated to age-remodeled nucleosomes

Remodeled nucleosomes with decreased (A) or increased (B) H3 occupancy with aging were given as inputs to the GREAT annotation portal. Results from the MSigDB transcription factor target annotation type are shown. Only annotations significant in 4 of the 5 tissues with FDR $<10^{-6}$ are reported. See also **Supplementary Table S3** for other significant annotations, including to Gene Ontology terms.

Supplementary Figure Legends

Figure S1: Remodeling of H3 nucleosomal occupancy with mouse aging in four tissues and one cell type.

(A) Heatmap of H3 ChIP signal centered on regions called as increased or decreased with aging. Note the increased or decreased signal at these called sites. (B-E) CEAS Genome ontology analysis in each tissue for nucleosomes with decreased (B) or increased (C) H3 occupancy during mouse aging, compared to all detected nucleosomes (D), or to the whole genome background (E).

Figure S2: Analysis of histone protein levels in aging samples by Western blot.

(A-B) Western blots for Vinculin, H3, and H2B from livers (A) and cerebellum (B) of aging male mice (5 *vs.* 21 months). Liver samples for H3 Western blotting were run on a 10% SDS-PAGE gel, and all other samples on a 4-20% SDS-PAGE precast gradient gel. To account for variability in protein extraction efficiency, 2 tissue pieces from each animal were used for independent protein extractions (technical duplicates). They are denoted as "extraction 1" and "extraction 2" in the figure for each cohort. Homogeneous protein loading was assessed by Coomassie brilliant blue staining. Note that the paired Vinculin and histone protein blots come from the same membrane that was cut based on an intermediate molecular weight prior to overnight primary antibody incubation. For ease of reading, the liver H2B and paired Vinculin raw blots have been "mirrored" in (A) to match the sample ordering of the same samples in the corresponding H3 blots, since the orientation of the gel for the transfer step was in the opposite direction. (C) H3 western blots for cerebellum and liver samples were run on the same 15% polyacrylamide gel for comparison of band migration. Apparent molecular weight differences for the H3 bands between cerebellum and liver samples in (A) and (B) appear to be due to differences in separating gels. Note that a faster migrating band can be observed in some H3 western blots. This band is generally fainter than the higher H3 molecular weight band observed, and may correspond to previously reported H3 cleavage [51, 52].

Figure S3: Analysis of histone protein levels in human senescent fibroblasts.

(A) Representative SA-β-galactosidase signal staining on IMR-90 and WI-38 cultures from an experiment paired with the protein extractions in (B). Senescence was induced by exposure to 250nM Doxorubicin for 24h [41, 42], and cells were left to recover for 14 days prior to SA-β-

galactosidase staining or protein extraction. Note the characteristic blue stain, which is indicative of a senescence phenotype. (B) Western blots for Vinculin and H3 from three human fibroblast cell lines: IMR-90, WI-38, and primary human dermal fibroblasts [HDF]. All samples were run on 4-20% SDS-PAGE gradient gels. Proliferating cell samples are denoted as "P", senescent cell samples are denoted as "S". Homogeneous protein loading was assessed by Coomassie brilliant blue staining. (C) Quantification of H3 relative protein intensity using Western Blots in proliferating (P) vs. senescent (S) human fibroblasts (normalized to cognate Vinculin loading control). Results are reported normalized to the respective intensity of the Vinculin band, and then, to account for cell-line specific differences in absolute protein levels, to the median value in the cognate cell line (each cell line is represented by dots in a different color). P-values reported above boxplots were obtained with the non-parametric Mann-Whitney/Wilcoxon test.

Figure S4: Analysis of H3 RNA transcript levels in aging mouse samples from RNA-seq data.

(A-E) Expression by RNA-seq of H3-encoding genes in heart (A), liver (B), cerebellum (C), olfactory bulb (D) and primary NSC cultures (E). The gene-level data was extracted from the previously published analysis of these samples [22]. Only H3-encoding genes with detectable RNA-seq reads are plotted, as the DEseq2 guidelines recommend removing undetectable genes from downstream analyses. Note that there is no general rule as to increased or decreased transcript levels for histone H3-encoding genes in these tissues.

Figure S5: Analysis of H3 ChIP-seq reads mapping to mouse *vs.* drosophila genome.

(A) Reads were mapped to the mouse mm9 build or the drosophila dm3 build, to discriminate reads derived from the chromatin of the aging mouse tissue (*i.e.* mapping to the mm9 genome) and the reads derived from the spiked-in S2 cell chromatin (*i.e.* mapping to the dm3 genome) in the previous ChIP-seq dataset [22]. Each dot on the plot represents one ChIP-seq sample. The reported value represents the relative number of reads mapping to the mouse genome divided by that mapping to the fly genome, then normalized to the average value of the 2 young samples for ease of interpretation. Thus, if no change in chromatin H3 levels occur with aging, all values will be at 1. If there is a decrease in H3 loaded onto chromatin with aging, values will reliably drop

below 1. If there is an increase in H3 loaded onto chromatin with aging, values will reliably rise above 1.

Figure S6: Model parameters for genome-wide chromatin state learning with ChromHMM. (A) Emission parameters of the trained model, and predicted function based on enriched histone marks. (B) Transition parameters of the trained model. (C-G) Enrichment of various genomic features for the different learned states.

Index of Supplementary Tables (Excel files)

Supplementary Table S1: Annotation of age-remodeled nucleosomes with respect to genomic elements and chromatin states.

Supplementary Table S2: Accession numbers of public datasets reanalyzed in this manuscript.

Supplementary Table S3: Significantly enriched ontology terms associated to regions of increased or decreased H3 occupancy with aging using GREAT. Only annotations significant in 4 of the 5 tissues, with FDR $<10^{-6}$ are reported.

Figure 1

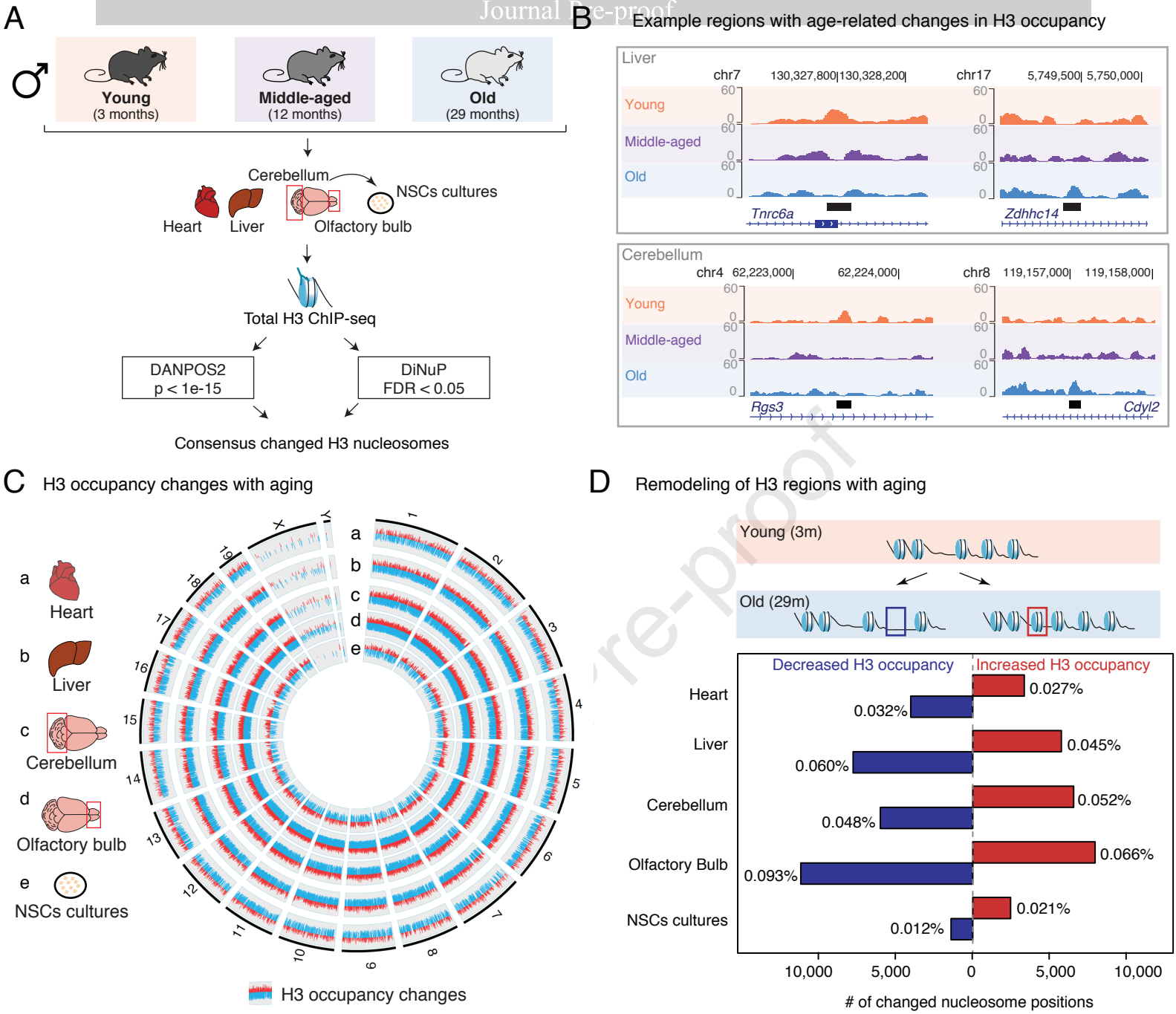

Figure 2

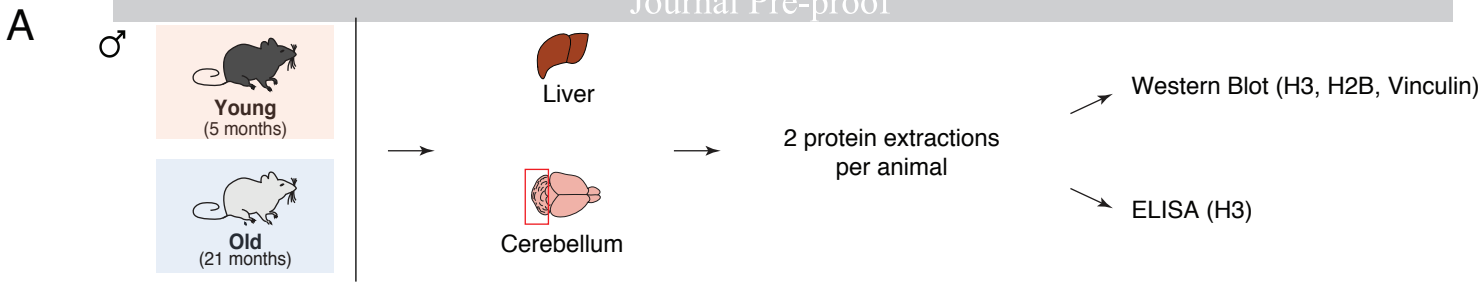

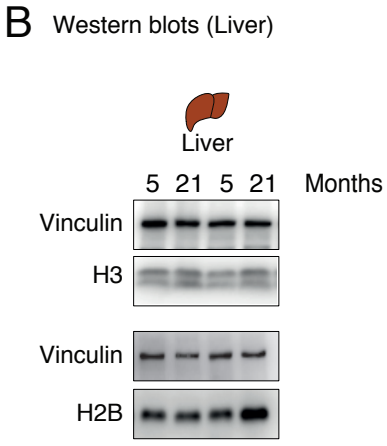

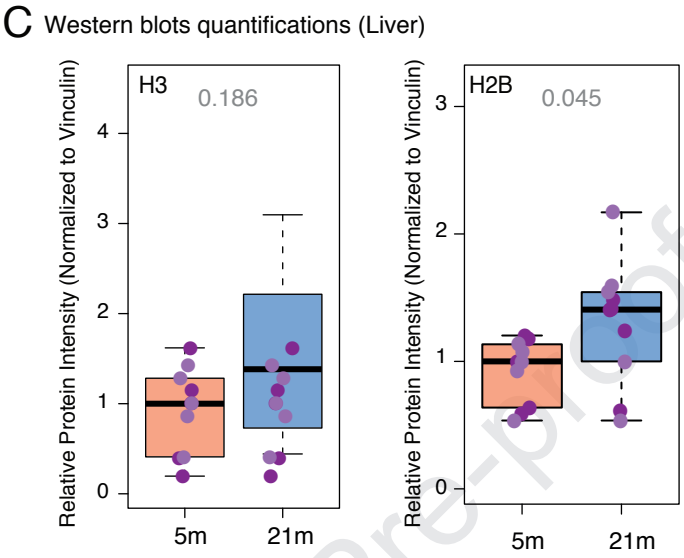

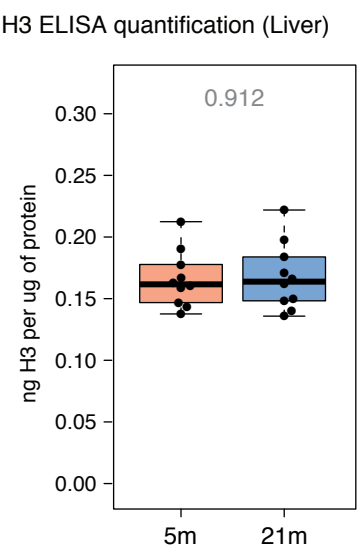

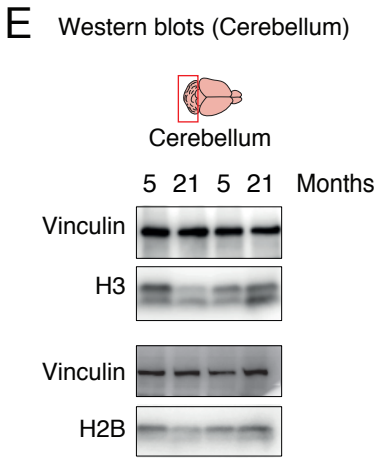

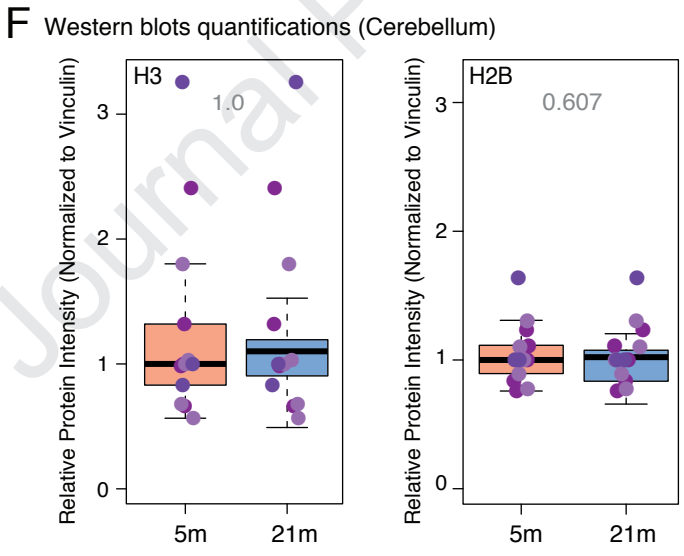

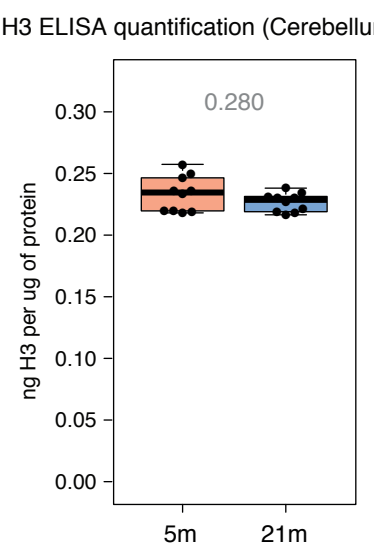

Figure 3

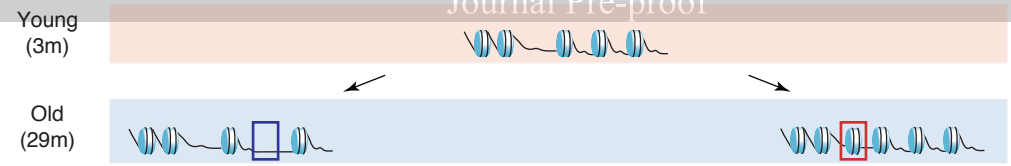

A Genomic distribution of regions with **decreased** H3 occupancy

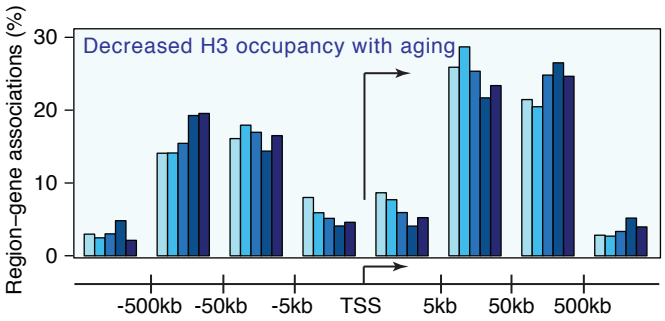

B Genomic distribution of regions with **increased** H3 occupancy

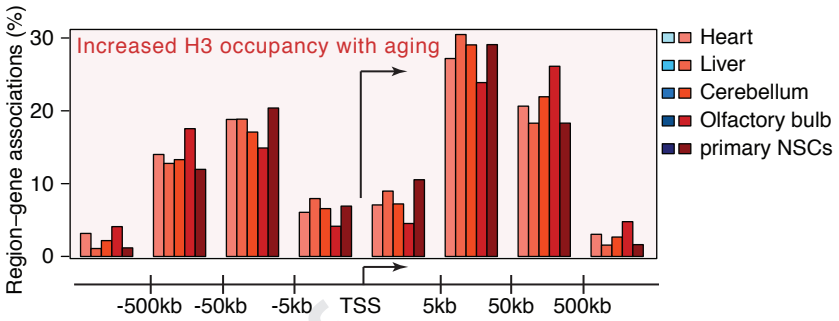

C Genomic annotations of regions with **decreased** H3 occupancy

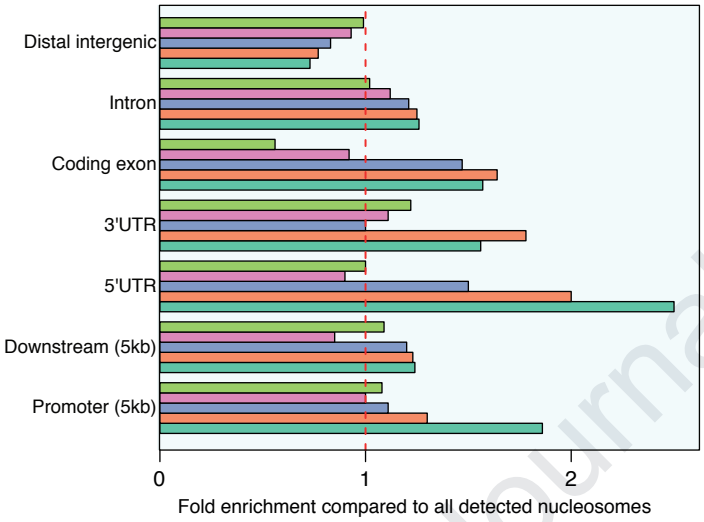

D Genomic annotations of regions with **increased** H3 occupancy

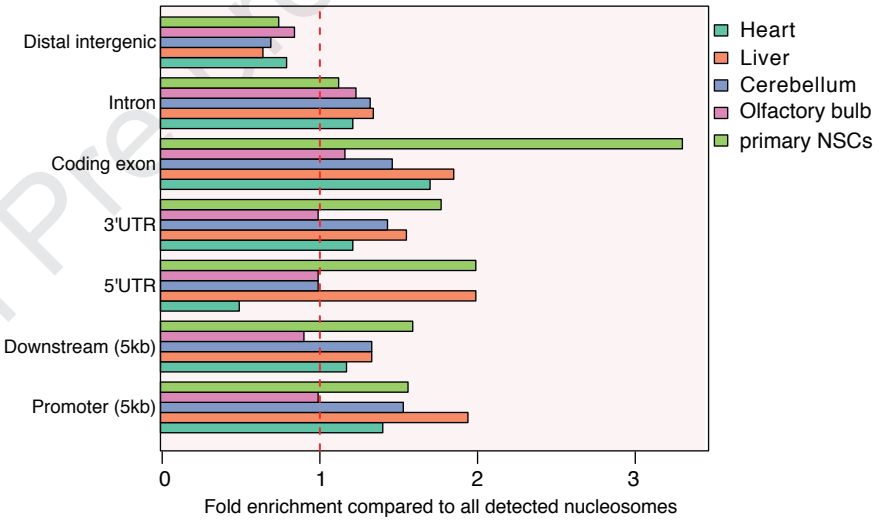

Figure 4

A MSigDB Predicted Promoter Motifs enrichment at regions of **decreased** H3 occupancy with aging (FDR <1E-06)

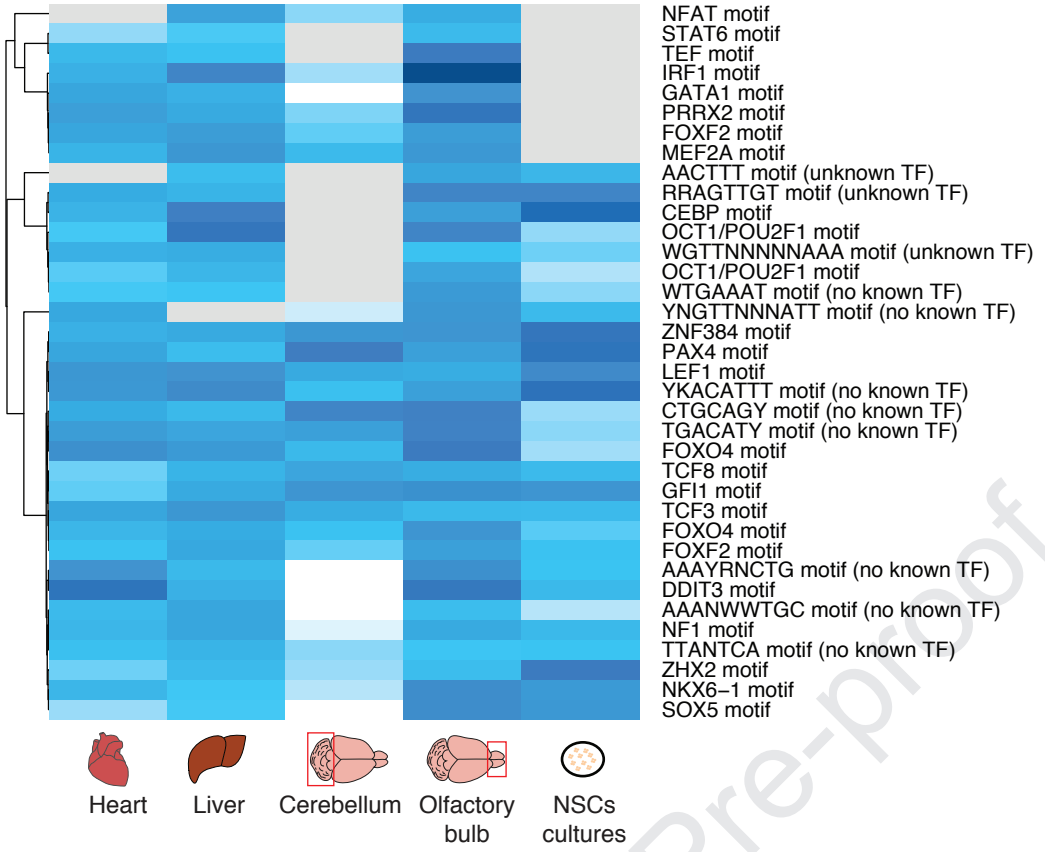

B MSigDB Predicted Promoter Motifs enrichment at regions of **increased** H3 occupancy with aging (FDR <1E-06)

Conflict of interest

The authors declare that they have no conflict of interest to disclose.